

Disruption of Lipid Uptake in Astroglia Exacerbates Diet Induced Obesity

Yuanqing Gao^{1,6}, Clarita Layritz¹, Beata Legutko¹, Thomas O Eichmann², Elise Laperrousaz³, Valentine S Moullé³, Celine Cruciani-Guglielmacci³, Christophe Magnan³, Serge Luquet³, Stephen C Woods⁴, Robert H Eckel⁵, Chun-Xia Yi^{1,6}, Cristina Garcia-Caceres¹, Matthias H Tschöp^{1*}.

¹Helmholtz Diabetes Center (HDC) & German Center for Diabetes Research (DZD), Helmholtz Zentrum München & Division of Metabolic Diseases, Technische Universität München, Munich, Germany.

²Institute of Molecular Biosciences, University of Graz, Austria.

³Unité de Biologie Fonctionnelle et Adaptative, Sorbonne Paris Cité, CNRS UMR 8251, University of Paris Diderot, Paris, France

⁴Department of Psychiatry and Behavioral Neuroscience, University of Cincinnati, USA.

⁵Division of Endocrinology, Metabolism, & Diabetes, University of Colorado at Denver, USA.

⁶Department of Endocrinology and Metabolism, Academic Medical Center, University of Amsterdam, The Netherlands

* Corresponding author:

Matthias H. Tschöp M.D.

Helmholtz Diabetes Center, Helmholtz Zentrum München

Parkring 13, 85764 Neuherberg, Germany

Tel: +49 89 31872044

tschoep@helmholtz-muenchen.de

words: 3828 figure: 5 Key words: astrocyte; diet induced obesity; lipoprotein lipase

Abstract

Neuronal circuits in the brain help to control feeding behavior and systemic metabolism in response to afferent nutrient and hormonal signals. Although astrocytes have historically been assumed to be less relevant for such neuroendocrine control, we asked whether lipid uptake via lipoprotein lipase (LPL) in astrocytes is required for the central regulation of energy homeostasis. *Ex vivo* studies with hypothalamic-derived astrocytes showed that LPL expression is up-regulated by oleic acid; whereas it is decreased in response to palmitic acid or triglyceride. Likewise, astrocytic LPL deletion reduced the accumulation of lipid drops in those glial cells. Consecutive *in vivo* studies showed that the postnatal ablation of LPL in glial fibrillary acidic protein (GFAP)-expressing astrocytes induced exaggerated body weight gain and glucose intolerance in mice exposed to a high-fat diet (HFD). Intriguingly, astrocytic LPL deficiency also triggered increased ceramide content in the hypothalamus, which may contribute to hypothalamic insulin resistance. We conclude that hypothalamic LPL functions in astrocytes to ensure appropriately balanced nutrient sensing, ceramide distribution, body weight regulation and glucose metabolism.

Introduction

Metabolic homeostasis is regulated by a complex central nervous system (CNS) network that senses and integrates nutrient and hormonal signals from the periphery to regulate feeding behavior, energy expenditure and glucose homeostasis. Considerable evidence indicates that lipid sensing by the brain is a normal component of such regulation [1-6], and the mechanism underlying brain lipid sensing's role in metabolism has attracted considerable interest in the metabolic field in recent years.

Glial cells constitute around 50% of the total cells in the whole brain [7], but until recently have historically received less attention in metabolic research. Astrocytes are the most abundant and diverse glial cells and they are the primary cell population in the brain that synthesizes and metabolizes lipids [8, 9], positioning them as major players in the regulation of lipid sensing and metabolism in the CNS. Consistent with this, fatty acid oxidation in the brain, although at a very low rate compared to glycolysis, occurs primarily in astrocytes [8, 10]. Further, chronic consumption of a HFD results in both hyperlipidemia and hypothalamic astrogliosis [11]. However, until now, the functional significance of astrocyte lipid metabolism in CNS metabolic regulation has been unknown.

Lipoprotein lipase (LPL) - the key enzyme to hydrolyze triglyceride -, has been implicated in CNS metabolic regulation [12]. LPL is the "gate-keeper" for lipids in peripheral tissues, modulating the distribution of fatty acids derived from TG-rich lipoproteins [13]. Importantly, LPL is regulated by nutrients and hormones in a tissue-specific manner [14]. LPL expression and enzyme activity have been detected in the brain in both neurons and glial cells [12, 15-17]. However, the functional significance of LPL in astrocytes is unknown.

In the current studies, we investigated the function of LPL in astrocytes in brain-lipid metabolism and potential contributions of astrocytic LPL to diet-induced obesity (DIO). We found that in astrocytes, LPL is responsible for controlling cellular lipid storage. In a loss-of-

function study, mice lacking LPL uniquely in astrocytes had glucose intolerance and accelerated body weight gain when maintained on a HFD. We also found increased ceramide content in the hypothalamus of astrocytic LPL-deficient mice, accompanied by increased microglial reactivity and endoplasmic reticulum (ER) stress. Collectively, our data imply that LPL in astrocytes mediates lipid partitioning in the brain, and that it is required for appropriate CNS nutrient sensing and the regulation of energy homeostasis.

Research Methods and Design

Animals

All studies were approved by and performed according to the guidelines of the Institutional Animal Care and Use Committee of the University of Cincinnati and the Institutional Animal Care and Use Committee of the Helmholtz Center Munich, Bavaria, Germany. All mice were group housed on a 12-h light dark cycle at 23°C, with free access to food and water. Mice were fed either a standard chow diet, or a HFD (D12331; Research Diets).

Astrocyte-specific postnatal LPL-knockout mice (GFAP-LPL^{-/-}) were generated by crossing the LPL^{lox/lox} mice [18] with hGFAP-CreER^{T2}, a transgenic mouse harboring the tamoxifen-inducible Cre recombinase driven by a human glial fibrillary acidic protein promoter (hGFAP) [19]. At the age of 6 wk, tamoxifen was given by IP injection for 5 consecutive d at a dose of 100 ug/d. LPL loxP-homozygous and Cre-positive mice were used to generate knockout mice (GFAP-LPL^{-/-}). Their littermates, which were LPL loxP-homozygous but Cre negative, served as WT controls (GFAP-LPL^{+/+}).

For the flow cytometry study, co-localization of ceramide in GFAP-positive astrocytes and the *in-situ* hybridization study, GFAP-LPL^{+/+} and GFAP-LPL^{-/-} mice were crossed with hGFAP-eGFP reporter mice [20] to label the Cre-targeted cells with an eGFP tag. To

evaluate the efficiency of the post-natal deletion in different brain regions, GFAP-LPL^{+/+} mice were crossed with Rosa26 ACTB-tdTomato reporter mice and received tamoxifen injection in the same way as the experimental group. To evaluate the presence of ceramide in microglia, we used microglia-GFP reporter mice (Jax mice 005582).

Hypothalamic Primary Culture

For astrocytes, hypothalami were isolated from 2-d-old C57BL6J mice and triturated in MEM containing 1% penicillin-streptomycin, 10% fetal calf serum and 5.5 mM glucose. The cell pellet was centrifuged, re-suspended and seeded in a 175-cm³ cell culture flask. After 8-9 d, the mixed glial culture reached 90% confluency. Then the flasks were placed in a 37°C shaking incubator at 240 rpm overnight to remove microglia. The cells were then seeded for the experiments.

For neurons, the hypothalami were isolated from 14-d embryos. After trypsinization, single cells were plated on 12-well plates and cultured in neurobasal medium supplemented with B-27 and GlutaMAX I. After 7 days in culture, the presence of glia cells were efficiently reduced through adding mitotic inhibitor Ara C (cytosine-1-β-D-arabinofuranoside), and hypothalamic neurons started to develop synaptic processes. Cells were then harvested to store at -80°C until RNA extraction.

Adenovirus Cre-mediated deletion of LPL in hypothalamic astrocyte cultures

To induce the *ex vivo* ablation of LPL, primary hypothalamic astrocytes were obtained from LPL^{lox/lox} mice and were seeded in 6-well cell culture plates as described above. Once they reached 90% confluency, astrocytes were transfected with adeno-Cre and adeno-control virus (Vector biolabs) plus 1% adenoboost (ATCGbio Life Technology) for 4 h to generate astrocyte cultures with LPL (Astro-LPL^{+/+}) or without LPL (Astro-LPL^{-/-}).

Seahorse analysis

Astrocytes were seeded in an XF24 plate (Seahorse Bioscience) with 80,000 cells per well. 24 h after adeno-cre or control virus transfection, cells were washed with PBS and incubated with XF assay medium containing 5.5 mM glucose for 1 h in a 37°C air incubator. The XF24 plate was then transferred to a temperature-controlled (37°C) extracellular flux analyzer (Seahorse Bioscience) and subjected to an equilibration period. For the analysis of extracellular acidification rates (ECARs) derived from glycolysis, the measurements were ended by the addition of 2-deoxy-glucose (2DG; 100 mM). 2DG-sensitive PPR estimates the ATP production from glycolysis with a 1:1 ratio. To normalize respirometry readings to cell number per well, cells were stained with crystal violet after the flux experiment. L-Lactate from the astrocyte culture medium was assayed by EnzyChrom™ lactate assay kit (Bioassays System).

Lipase activity assay

Cells were collected in 20 mM Tris 150 mM NaCl with 15 ug/ml heparin. After sonication, cell lysates were kept at 37°C for 45 min, following by 10,000 g centrifuge at 4°C for 10 min. Lipase activity was determined by a fluorometric lipoprotein lipase activity assay kit (STA-610-CB, cell biolabs). Protein level was determined by a BCA assay. Lipase activity was normalized to protein content.

Real-time PCR

For gene expression analysis, hypothalamic tissue was harvested and total RNA was isolated by an RNeasy lipid tissue kit (Qiagen). After reverse transcription by a QuantiTect Rev. Transcription Kit (Qiagen), gene expression was analyzed by a real-time PCR with Taqman probes (Applied Biosystems) and SYBR primers. Hypoxanthine phosphoribosyltransferase 1

(HPRT) was used as a housekeeping gene. Sequences information can be found in Table.1 (Supplemental information).

PCR

For PCR to detect the LPL delta band after Cre-loxP recombination, sequences of primers were set as follows: Forward 5'-CGCCCTGGAACATCACTAAT-3'; Reverse: 5'-CTTCTCAATTGT GGCAGGT-3'. The primers would develop a band of about 2000 bp on WT DNA sequence and a LPL delta band of 409 bp after floxed sequences cut by Cre.

Flow cytometry

The isolation protocol has been described in detail before [21]. Briefly, the forebrain was dissected and dissociated by enzymatic and mechanical approaches. Single cells were separated by sucrose gradient. Sorting was done by a flow cytometry cell sorter: FACS Aria I with FACS Diva software (BD Biosciences) based on GFP signals. Purified GFAP-expressing astrocytes from GFAP-LPL^{+/+} and GFAP-LPL^{-/-} mice were used for validating the LPL knock-down by real-time PCR as described above.

Glucose Tolerance Test

An intraperitoneal glucose tolerance test (ipGTT) was performed by injection of glucose (2 g/kg, 25% wt/vol. d-glucose (Sigma) in 0.9% wt/vol NaCl after a 5-h fast. Tail blood glucose levels (mg/dl) were measured with a TheraSense Freestyle glucometer (Abbott Diabetes Care) before (0 min) and at 15, 30, 60 and 120 min after injection.

Feeding experiments and metabolic phenotyping

Body weight were measured weekly through the study. Food intake was measured on a daily basis for two wk at the end of the study. Animals were double-housed and daily food intake of each cage was measured and averaged to per mice per day. Measurements of energy expenditure and physical activity were performed by a customized indirect calorimetric system (TSE Systems). Mice were adapted to the system for 24 h before data collection for the following 4 d.

Immunohistochemistry and Image Analysis

Immunohistochemistry was carried out as described before [22]. Briefly, mice were perfused and fixed by 4% paraformaldehyde in 0.1 M PBS (pH 7.4) at 4°C. After being equilibrated for 48 h with 30% sucrose in TBS, coronal sections (30 µm) were cut on a cryostat. Sections were washed and incubated with primary antibodies at 4°C overnight: rabbit anti-GFAP (DAKO), rabbit anti-iba1 (synaptic systems), mouse anti-ceramide (Enzo life science), rabbit anti-NeuN (cell signaling). On the second day, sections were rinsed and incubated with biotinylated secondary antibodies and avidin-biotin complex (Vector Laboratories). The reaction product was visualized by incubation in 1% diaminobenzidine with 0.01% hydrogen peroxide. For immunofluorescence, sections were incubated with corresponding alexa fluorescent secondary antibodies (Jackson ImmunoResearch).

Immunoreactivity was analyzed by ImageJ. Appropriate color threshold for DAB staining was set up manually for the first picture and applied to all the rest pictures. The brain area covered by the DAB staining signals (iba1, GFAP and AGRP) above the color threshold of each individual brain section in the fixed hypothalamic region was used to quantify the immunoreactivity. Two brain sections (at the similar anatomical level) of each individual animal were used to calculate the immunoreactivity average of each animal.

***In-situ* hybridization**

For in-situ hybridization, 30-um coronal sections were treated with 2 ug/ml proteinase K 30 min at 37°C, 0.2% glycine buffer 30 s and 0.1% Triton X-100 for 10 min. Brain sections were hybridized in hybridization buffer (Sigma-Aldrich) containing 200 nM locked nucleic acid (LNA) – modified cDNA probes labelled with digoxigenin (5'-TGGAAGTACTTCTCTAACATAT-3') (Exiqon) at 52 °C overnight. After stringent washing in SSC buffer in 52 °C and final washing in 0.1 M PBS, the sections were co-incubated with goat anti-digoxigenin antibody (Abcam) and chicken anti-GFP (Acris) at 4 °C overnight. Sections were incubated with biotinylated anti-chicken secondary antibody for 1 h and then incubated with streptavidin conjugated with DyLight 488 (for GFP) and rabbit anti-chicken antibody conjugated by Dylight 647 (for digoxigenin) (all from Jackson ImmunoResearch Laboratories). After thorough rinsing, the sections were mounted with mounting medium and visualized by confocal microscopy (Zeiss-LSM710).

Untargeted lipidomic analysis of ceramide species

Total lipids of weighed hypothalamus preparations were extracted twice according to Folch et al. [23], using chloroform/methanol/water (2/1/0.6, v/v/v) containing 500 pmol butylated hydroxytoluene, 1% acetic acid, and 4 nmol C17-ceramide as internal standard (ISTD, Avanti Polar Lipids) per sample. Combined organic phases of the double-extraction were dried under a stream of nitrogen and dissolved in 200 µl chloroform/methanol/2-propanol (2/1/12, v/v/v) for UPLC-qTOF analysis. Chromatographic separation was performed using an AQUITY-UPLC system (Waters Corporation), equipped with a HSS T3 column (2.1x100 mm, 1.8µm; Waters Corporation) as previously described [24]. A SYNAPT™G1 qTOF HD mass spectrometer (Waters Corporation) equipped with an ESI source was used for detection. Data

acquisition was done by the MassLynx 4.1 software (Waters Corporation). Ceramides were analyzed with the “Lipid Data Analyzer 1.6.2” software. Extraction efficacy and lipid recovery was normalized using ISTDs.

Statistical Analysis

All statistical analyses were performed using GraphPad Prism. Two groups were compared by using two-tailed unpaired Student’s t test. Two-way ANOVA was performed to detect significant interactions between genotype and diet, and multiple comparisons were analyzed following Bonferroni’s post hoc tests. P values lower than 0.05 were considered significant. All results are presented as means \pm SD when $n < 10$, as means \pm SEM when $n > 10$.

Results

Astrocytic LPL is regulated by nutrients in the hypothalamus

LPL activity has been detected in the hypothalamus, with changes occurring in response to a prolonged fast [25]. We first confirmed the presence of LPL in the hypothalamus, and particularly in primary astrocytes, as well as its modulation in response to different nutrient stimuli. Consistent with previous reports, LPL was expressed by both neurons and glial cells [12, 26]. We compared the relative abundance of LPL in primary isolated hypothalamic neurons and astrocytes, and found higher enriched-LPL mRNA levels in astrocytes than in neurons (Fig. 1A). Next, we evaluated the impact of the exposure to lipid on LPL expression *in vivo* and *in vitro*. An increase in LPL mRNA levels was observed in the hypothalamus of 8-mo HFD-fed mice (Fig. 1B). When hypothalamic-derived astrocytes were exposed to triglyceride (TG) and palmitic acid, LPL expression was reduced, whereas the opposite effect was seen with oleic acid (Fig. 1C&D). These data suggest that astrocytic LPL is regulated by nutrients and responds differentially to saturated versus non-saturated fatty acids.

The loss of LPL reduces cellular lipid content and increases glycolytic capacity in a hypothalamic astrocyte culture.

To analyze whether LPL in astrocytes regulates cellular lipid accumulation and glucose metabolism, we isolated hypothalamic astrocytes from LPL^{lox/lox} mice and performed virus-mediated excision of LPL by *in vitro* transfection with Cre-expressing adenoviruses (AAV-Cre), to finally obtain astrocytes with (Astro-LPL^{+/+}) and without LPL (Astro-LPL^{-/-}). A reduction of LPL expression (Fig. 2A) and lipase activity (Fig. 2B) were confirmed by qPCR and the lipase activity assay, respectively, after virus transfection. Loss of LPL activity leads to a decrease of lipid droplet content in astrocytes as assessed by Oil red O staining (Fig. 2C). Lipogenesis-related genes including cluster of differentiation 36 (CD36) and fatty acid synthase (FASN) were upregulated in LPL-deficient astrocytes (Fig. 2A), indicating a compensatory response to the lipid-derived situation. We next determined whether LPL regulates glycolysis in astrocytes (Fig. 2D). Indeed, Astro-LPL^{-/-} cells had increased cellular acidification and maximal glycolytic capacity (Fig. 2E&F). More ATPs were produced from enhanced glycolysis compared with what occurred in Astro-LPL^{+/+} (Fig. 2G). Accordingly, lactate secretion was increased in the medium from Astro-LPL^{-/-} (Fig. 2H), consistent with the increased glycolysis. These data indicate that LPL participates in regulating lipid content and energy metabolism in astrocytes. Specifically, we found that the lack of LPL reduces astrocytic lipid storage and enhances astrocytic glycolysis.

Validation of postnatal ablation of LPL in GFAP-expressing cells in the brain

To evaluate the impact of the loss of LPL in astrocytes *in vivo*, we generated postnatal astrocyte-specific LPL-knockout mice by the Cre/lox system. We first validated the deletion of LPL in astrocytes after peripheral tamoxifen injection at 6 wk of age by multiple

approaches. We confirmed the Cre-driven deletion of LPL in hGFAP positive cells by *in-situ* hybridization (Fig.3A). Primers were designed based on genetic construction of LPL-floxed sequences to detect a specific band after Cre-induced recombination (Fig. 3B). Purified GFAP-expressing astrocytes were sorted from the brain of GFAP-LPL^{+/+} (LPL^{lox/lox} mice injected with tamoxifen) or GFAP-LPL^{-/-} mice (hGFAP-CreER^{T2}-LPL^{lox/lox} injected with tamoxifen), which were crossed with hGFAP-eGFP reporter mice. qPCR of sorted brain GFP-expressing cells confirmed the knockdown of LPL (Fig. 3C). Using Rosa26 ACTB-ttdTomato reporter mice which were crossed with GFAP-LPL^{-/-} mice, we confirmed that Cre-mediated postnatal ablation occurred in the brain after tamoxifen injection, (Fig. S1A). The majority of the Cre-recombined GFAP-expressing astrocytes were located in the hypothalamus (46.3% ± 2.1%) in comparison with other brain regions such as thalamus, hippocampus and cortex (Fig. 3D). Even though GFAP is also expressed in peripheral tissues including stellate cells in liver and pancreas [27, 28], no alterations in LPL expression were found in the liver between GFAP-LPL^{+/+} and GFAP-LPL^{-/-} mice (Fig. 3E). Glucose-induced insulin secretion in isolated islets was also not affected between groups (Fig. 3F). These findings confirm that the loss of LPL occurs specifically in GFAP-expressing cells in the brain.

The loss of LPL in astrocytes causes ceramide accumulation, microglial activation and increased Agouti-related peptide (AGRP) in the hypothalamus and not in other brain areas

Previously, it has been reported that ceramide synthesis in the brain is associated with LPL activity [29]. Ceramide is an important multi-functional intracellular signaling molecule. In the periphery, ceramide accumulation causes lipid toxicity and insulin resistance [30, 31]. In the mouse brain, after knocking out LPL from GFAP-positive astrocytes, total ceramide

content was increased in the hypothalamus (Fig. 4A). Ceramide species having different acyl-chains were also analyzed (Fig. 4B). Mice lacking astrocytic LPL had increased C18:0, C18:1 and C22:0 levels in the hypothalamus. By ceramide staining, we also found that ceramide immunoreactivity (-ir) positive cells, which are mainly neurons (Fig. S2), were markedly increased in GFAP-LPL^{-/-} mice in the hypothalamus (Fig. S1B&C), consistent with the lipidomics results.

In accordance with several studies that have reported that ceramide accumulation in the hypothalamus causes endoplasmic reticulum (ER) stress and interrupts energy balance [32], we observed that the loss of LPL in astrocytes increased the expression of several ER stress markers in the hypothalamus. Specifically, we found that chaperone GRP78 (glucose-regulated protein 78 kDa), total Xbp1 (X-box binding protein 1) and sliced Xbp1 (sXbp1), were each increased in the hypothalamus of GFAP-LPL^{-/-} mice (Fig. 4C); whereas were unchanged in the hippocampus or cortex of those mice (Fig. S1F-G).

We also analyzed the effect of the loss of LPL in astrocytes by immunohistochemistry. GFAP immunoreactivity did not differ between GFAP-LPL^{+/+} and GFAP-LPL^{-/-} mice (Fig. 4D&E). On the other hand, the major immune responsive cells – microglia, had increased reactivity in GFAP-LPL^{-/-} mice medial basal hypothalamus (Fig. 4F&G), but not in other brain regions (Fig. S1D&E), suggesting that microglia responded to the ceramide-induced lipid toxicity, and that this may contribute to the hypothalamic insulin resistance and metabolic disorders. Such glial and ceramide alterations in the hypothalamus were associated with changes in specific neuronal populations involved in the regulation of energy balance: AGRP neurons and Proopiomelanocortin (POMC) neurons. While POMC cell number did not change (Fig.

4H&I), AGRP immunoreactivity was significantly elevated in the GFAP-LPL^{-/-} mice (Fig. 4J&K).

Collectively, these data suggest that in the current model, lack of LPL in astrocytes causes ceramide accumulation in hypothalamus, and is associated with microglial activation, ER stress and increased AGRP.

Mice lacking LPL in astrocytes have exaggerated body weight gain and glucose intolerance when maintained on HFD diet.

To assess whether the loss of LPL in astrocytes affects whole-body energy metabolism, mice were maintained on chow or HFD for 10 wk beginning at 10 wk of age. Only modest metabolic phenotypes were initially observed when the animals were fed the chow diet (see Fig. S3). Briefly, GFAP-LPL^{-/-} mice exhibited a glucose intolerance phenotype and reduced activation of AKT (phospho-AKT; phosphorylation in Ser 473 of protein kinase B) in the hypothalamus 10 min after peripheral insulin stimulation. Although the mice had a slightly higher food intake at 24 wk of age compared with GFAP-LPL^{+/+} mice, no changes were detected in body weight or fat mass.

When these mice were fed with a HFD, GFAP-LPL^{-/-} mice had accelerated body weight gain (Fig. 5A) relative to controls, and this was mainly due to increased fat mass (Fig. 5B&C). Calorimetric measurements after 10 wk on the HFD revealed that GFAP-LPL^{-/-} mice had increased food intake (Fig. 5D) and lower locomotor activity (Fig. 5F), and these likely contributed to the increased body weight gain. Higher energy expenditure (Fig. 5E) might be the consequence of the higher body weight of GFAP-LPL^{-/-} mice. Plasma leptin level was elevated in GFAP-LPL^{-/-} mice (Fig.5G), which was consistent with the increased fat mass.

Plasma insulin level did not change (Fig.5H). GFAP-LPL^{-/-} mice had enhanced glucose intolerance (Fig.5I&J). Since GFAP-LPL^{-/-} mice on the chow diet already exhibited glucose intolerance without changes in body weight or fat mass, we determined that the genotype is determinant of the glucose intolerance phenotype. In GFAP-LPL^{-/-} mice maintained with the HFD, the increased adiposity exaggerates the glucose intolerance. Thus, the loss of LPL in astrocytes induces a glucose intolerance and exaggerated body weight on a HFD, implying that LPL-related lipid metabolism in astrocytes has an important role in regulating metabolic homeostasis.

Discussion

In the present experiments, we investigated the function of LPL in astrocytes and its role in systemic metabolic control. We first found that LPL expression is increased in the hypothalamus of long-term HFD-fed mice, suggesting a potential role of LPL in the diet-induced obesity pathology. We also found that LPL is more abundant in astrocytes than in neurons, consistent with the classic view that CNS astrocytes actively consume lipid. We found that LPL controls lipid storage in astrocytes in response to different nutrient inputs. A lack of LPL in astrocytes resulted in exaggerated body weight gain and glucose intolerance in animals fed a HFD, and these phenotypes were associated with increased ceramide content in the hypothalamus. These results indicate that astrocytes play a key role in TG sensing and the control of lipid homeostasis.

We found that the LPL level in astrocytes varies according to the amount and specific mix of extracellular lipids. LPL was down-regulated in the presence of TGs and palmitic acid, but up-regulated by oleic acid. These data suggest that LPL may protect astrocytes from saturated

fatty acid overload, an essential regulatory function for astrocytes to function properly during HFD-induced hyperlipidemia.

Moreover, we also observed increased ceramide content in the hypothalamus of mice lacking astrocytic LPL, consistent with studies indicating that the inhibition of LPL activity triggers *de novo* ceramide synthesis [29]. In our study, we found that the deletion of LPL from astrocytes resulted in ceramide accumulation in hypothalamic neurons. Given that astrocytes metabolically supply lipids to neurons [9, 33], we cannot rule out that the LPL deficiency in astrocytes might also cause the reduction of neuronal FA availability, triggering *de novo* ceramide synthesis in neurons as we observed. In our mouse model, we also found changes in AGRP immunoreactivity in the hypothalamus that might be a consequence of reduced lipid storage in the microenvironment due to the LPL deletion in astrocytes. Indeed, Libby *et al.*, reported that LPL is able to modulate AGRP level through the regulation of lipid storage in neurons [34]. Besides the ceramide-induced lipid toxicity, we also observed elevation of ER stress markers and increased microglial immunoreactivity in the hypothalamus, both of which are associated with ceramide accumulation as reported in other studies [31, 32]. Thus, these data suggest that disrupted lipid uptake in astrocytes causes ceramide accumulation and consequentially contributes to the pathology of obesity.

Compared with previous studies using neuronal LPL knockout approach [12], our astrocytic LPL-knockout mouse model had unchanged body weight on a chow diet. Given that LPL is highly expressed in the rat brain during the lactating period, and falls dramatically after weaning [35], we induced the deletion of LPL in adult mice to avoid developmental complications. Moreover, this deletion was restricted to GFAP-expressing astrocytes, which induced mainly changes in the hypothalamus rather than other brain areas, to investigate the

significance of LPL function in these glial cells in the adult stage.

Overall, our data highlight the role of astrocytic lipid uptake in energy homeostasis. Mice lacking LPL in astrocytes have disrupted lipid metabolism in astrocytes and ceramide accumulation in hypothalamic neurons, contributing to impaired glucose tolerance and accelerated body weight gain in animals fed a HFD.

Acknowledgement

The authors thank Carola Meyer and Elma Stapic (Helmholtz Diabetes Center) for the support of animal work organizing. The authors also appreciate the support from animal facility staff at University of Cincinnati (Metabolic Disease Institute) and Helmholtz Diabetes Center. This work was supported in part by funding to M.H.T from the Alexander von Humboldt Foundation, the Helmholtz Alliance ICAMED & the Helmholtz Initiative on Personalized Medicine iMed by Helmholtz Association, and the Helmholtz cross-program topic “Metabolic Dysfunction”. Moreover, this work also was supported by funding of European Research Council ERC (AdG HypoFlam no. 695054).

Author contributions

Y.G. performed the study, researched the data, analyzed results and wrote the manuscript. C.L. and B.L. performed the experiments. T.O.E. performed the lipidomic analysis. Y.G., E.L., V.S.M., C.C.G., C.M., S.L., R.H.E., C.X.Y., C.G.C. and M.H.T. participated in the design of the project and discussion. S.C.W., C.G.C. and M.T. were involved in the design and the writing of the manuscript. Authors had no relevant conflict of interest to disclose. M.H.T. is the guarantor of this work and had full access to all the data in the study and takes responsibility for the integrity of the data and the accuracy of the data analysis.

References:

1. Clement, L., et al., *Intracerebroventricular infusion of a triglyceride emulsion leads to both altered insulin secretion and hepatic glucose production in rats*. *Pflugers Arch*, 2002. **445**(3): p. 375-80.
2. Cruciani-Guglielmacci, C., et al., *Beta oxidation in the brain is required for the effects of non-esterified fatty acids on glucose-induced insulin secretion in rats*. *Diabetologia*, 2004. **47**(11): p. 2032-8.
3. Lam, T.K., et al., *Hypothalamic sensing of circulating fatty acids is required for glucose homeostasis*. *Nat Med*, 2005. **11**(3): p. 320-7.
4. Lopez, M., C.J. Lelliott, and A. Vidal-Puig, *Hypothalamic fatty acid metabolism: a housekeeping pathway that regulates food intake*. *Bioessays*, 2007. **29**(3): p. 248-61.
5. Obici, S., et al., *Central administration of oleic acid inhibits glucose production and food intake*. *Diabetes*, 2002. **51**(2): p. 271-5.
6. Oomura, Y., et al., *Effect of free fatty acid on the rat lateral hypothalamic neurons*. *Physiol Behav*, 1975. **14**(04): p. 483-6.
7. Azevedo, F.A., et al., *Equal numbers of neuronal and nonneuronal cells make the human brain an isometrically scaled-up primate brain*. *J Comp Neurol*, 2009. **513**(5): p. 532-41.
8. Edmond, J., *Energy metabolism in developing brain cells*. *Can J Physiol Pharmacol*, 1992. **70 Suppl**: p. S118-29.
9. Le Foll, C., et al., *Regulation of hypothalamic neuronal sensing and food intake by ketone bodies and fatty acids*. *Diabetes*, 2014. **63**(4): p. 1259-69.
10. Edmond, J., et al., *Capacity for substrate utilization in oxidative metabolism by neurons, astrocytes, and oligodendrocytes from developing brain in primary culture*. *J Neurosci Res*, 1987. **18**(4): p. 551-61.
11. Horvath, T.L., et al., *Synaptic input organization of the melanocortin system predicts diet-induced hypothalamic reactive gliosis and obesity*. *Proc Natl Acad Sci U S A*, 2010. **107**(33): p. 14875-80.
12. Wang, H., et al., *Deficiency of lipoprotein lipase in neurons modifies the regulation of energy balance and leads to obesity*. *Cell Metab*, 2011. **13**(1): p. 105-13.
13. Fielding, B.A. and K.N. Frayn, *Lipoprotein lipase and the disposition of dietary fatty acids*. *Br J Nutr*, 1998. **80**(6): p. 495-502.
14. Wang, H. and R.H. Eckel, *Lipoprotein lipase: from gene to obesity*. *Am J Physiol Endocrinol Metab*, 2009. **297**(2): p. E271-88.
15. Huey, P.U., et al., *Lipoprotein lipase is expressed in cultured Schwann cells and functions in lipid synthesis and utilization*. *J Lipid Res*, 1998. **39**(11): p. 2135-42.
16. Nishitsuji, K., et al., *Lipoprotein lipase is a novel amyloid beta (Abeta)-binding protein that promotes glycosaminoglycan-dependent cellular uptake of Abeta in astrocytes*. *J Biol Chem*, 2011. **286**(8): p. 6393-401.
17. Wang, H. and R.H. Eckel, *Lipoprotein lipase in the brain and nervous system*. *Annu Rev Nutr*, 2012. **32**: p. 147-60.

18. Augustus, A., et al., *Cardiac-specific knock-out of lipoprotein lipase alters plasma lipoprotein triglyceride metabolism and cardiac gene expression*. J Biol Chem, 2004. **279**(24): p. 25050-7.
19. Ganat, Y.M., et al., *Early postnatal astroglial cells produce multilineage precursors and neural stem cells in vivo*. J Neurosci, 2006. **26**(33): p. 8609-21.
20. Nolte, C., et al., *GFAP promoter-controlled EGFP-expressing transgenic mice: a tool to visualize astrocytes and astrogliosis in living brain tissue*. Glia, 2001. **33**(1): p. 72-86.
21. Fischer, J., et al., *Prospective isolation of adult neural stem cells from the mouse subependymal zone*. Nat Protoc, 2011. **6**(12): p. 1981-9.
22. Gao, Y., et al., *Hormones and diet, but not body weight, control hypothalamic microglial activity*. Glia, 2014. **62**(1): p. 17-25.
23. Folch, J., M. Lees, and G.H. Sloane Stanley, *A simple method for the isolation and purification of total lipides from animal tissues*. J Biol Chem, 1957. **226**(1): p. 497-509.
24. Knittelfelder, O.L., et al., *A versatile ultra-high performance LC-MS method for lipid profiling*. J Chromatogr B Analyt Technol Biomed Life Sci, 2014. **951-952**: p. 119-28.
25. Eckel, R.H. and R.J. Robbins, *Lipoprotein lipase is produced, regulated, and functional in rat brain*. Proc Natl Acad Sci U S A, 1984. **81**(23): p. 7604-7.
26. Nimmerjahn, A., F. Kirchhoff, and F. Helmchen, *Resting microglial cells are highly dynamic surveillants of brain parenchyma in vivo*. Science, 2005. **308**(5726): p. 1314-8.
27. Ding, Z., et al., *Glial fibrillary acidic protein promoter targets pancreatic stellate cells*. Dig Liver Dis, 2009. **41**(3): p. 229-36.
28. Tennakoon, A.H., et al., *Analysis of glial fibrillary acidic protein (GFAP)-expressing ductular cells in a rat liver cirrhosis model induced by repeated injections of thioacetamide (TAA)*. Exp Mol Pathol, 2015. **98**(3): p. 476-85.
29. Picard, A., et al., *Hippocampal lipoprotein lipase regulates energy balance in rodents*. Mol Metab, 2014. **3**(2): p. 167-76.
30. Chavez, J.A. and S.A. Summers, *A ceramide-centric view of insulin resistance*. Cell Metab, 2012. **15**(5): p. 585-94.
31. Holland, W.L., et al., *Lipid-induced insulin resistance mediated by the proinflammatory receptor TLR4 requires saturated fatty acid-induced ceramide biosynthesis in mice*. J Clin Invest, 2011. **121**(5): p. 1858-70.
32. Contreras, C., et al., *Central ceramide-induced hypothalamic lipotoxicity and ER stress regulate energy balance*. Cell Rep, 2014. **9**(1): p. 366-77.
33. Guzman, M. and C. Blazquez, *Is there an astrocyte-neuron ketone body shuttle?* Trends Endocrinol Metab, 2001. **12**(4): p. 169-73.
34. Libby, A.E., et al., *Lipoprotein lipase is an important modulator of lipid uptake and storage in hypothalamic neurons*. Biochem Biophys Res Commun, 2015. **465**(2): p. 287-92.
35. Tavangar, K., et al., *Developmental regulation of lipoprotein lipase in rats*. Am J Physiol, 1992. **262**(3 Pt 1): p. E330-7.

Figure legends

Figure 1. Astrocytic LPL is regulated by nutrients in the hypothalamus. Expression levels of LPL in primary isolated hypothalamic neurons and astrocytes (A) and the hypothalamus of mice fed HFD for 8 months (B). In primary astrocytes, LPL expression levels were modulated by 0.02% TG-emulsion (C), and 50 μ M of oleic acid, palmitic acid or BSA vehicle (D). LPL: Lipoprotein lipase. BSA: bovine serum albumin. TG: triglyceride. $p < 0.05$ for *. n=4-7 per group.

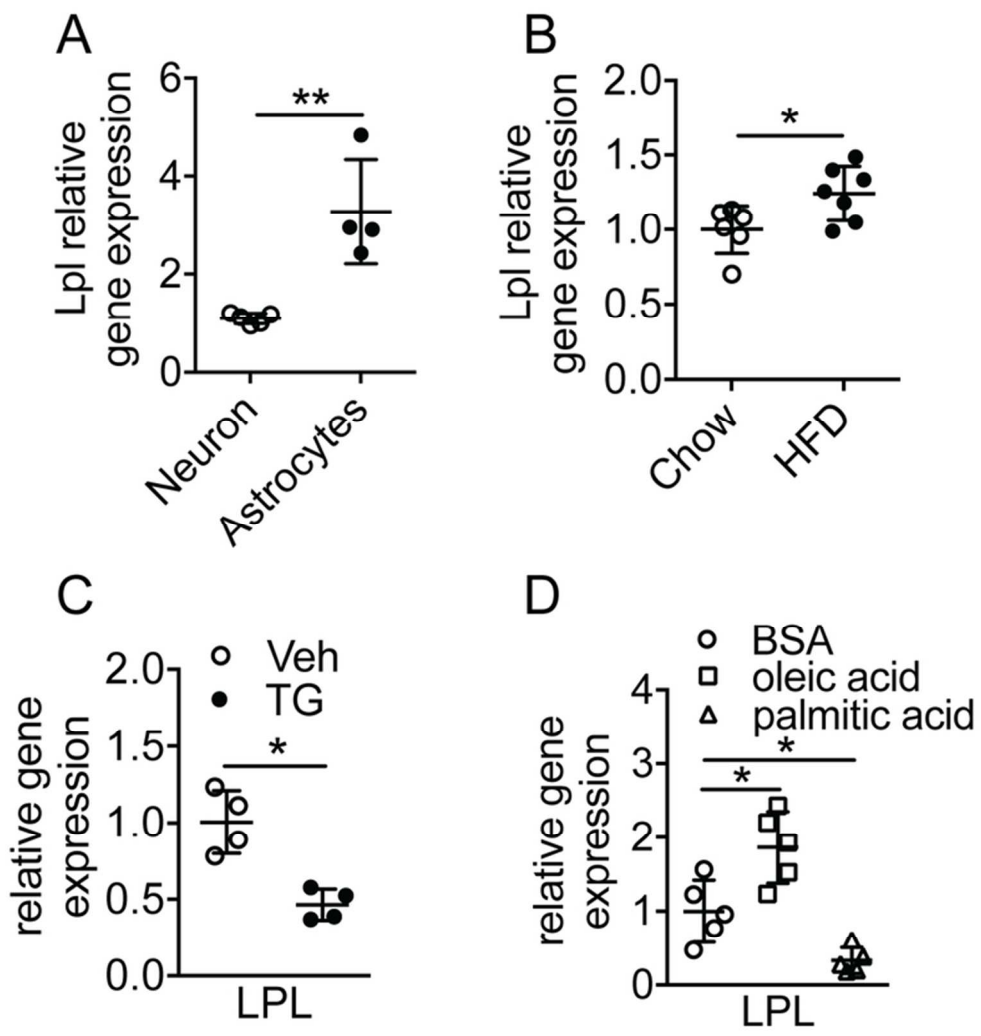
Figure 2. The loss of LPL reduces cellular lipid content and increases glycolytic capacity in hypothalamic astrocyte cultures. Astrocytes were isolated from hypothalami of LPL-flox mice and transfected with adeno-GFP or adeno-Cre virus to obtain astrocytes with LPL (Astro-LPL^{+/+}) or without LPL (Astro-LPL^{-/-}). The loss of LPL in astrocyte cultures induced changes in the expression of LPL, Fasn and Cd36 (A), lipase activity (B) and lipid content in astrocytes stained by Oil Red O (C). Seahorse analysis demonstrated that Astro-LPL^{-/-} had enhanced glycolysis (D&E), increased mitochondrial glycolytic capacity (F), and increased ATP production from glycolysis (G). Lactate secretion was also higher in Astro-LPL^{-/-} compared with Astro-LPL^{+/+} (H). Fasn: fatty acids synthase. Cd36: cluster of differentiation 36. ECAR: extracellular acidification rate. $p < 0.05$ for *, $p < 0.001$ for ***. Scale bar=50 μ m. n=5-6 per group.

Figure 3. Validation of postnatal ablation of LPL in GFAP-expressing cells in the mouse brain. Astrocyte-specific LPL postnatal KO mice were achieved by crossing GFAP-

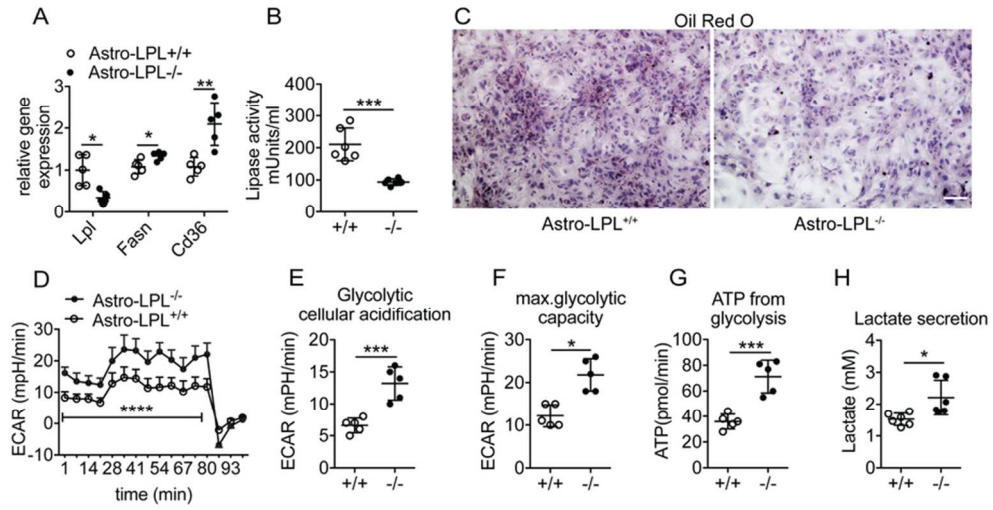
CreER^{T2+/-} with LPL flox^{+/+}. After tamoxifen injection at 6 wk of age, LPL deletion was confirmed by *in-situ* hybridization (A), PCR for DNA sequences after Cre-mediated the deletion of exon 1 in LPL gene (B), and qPCR from purified GFAP-positive astrocytes isolated by flow cytometry from GFAP-LPL^{+/+} and GFAP-LPL^{-/-} (C). Efficiency of Cre-mediated recombination was evaluated by crossing GFAP-LPL^{+/+} mice with Rosa26 ACTB-tdTomato reporter mice through the ratio between Cre-recombined astrocytes in different brain regions and the total Cre-recombined cells detected in brain slides (D). No differences in LPL expression were found in the liver (E) nor *ex vivo* insulin secretion from isolated islets in response to glucose (F). $p < 0.05$ for *: vs Astro-LPL^{+/+}. Scale bar=10 μ m. n=4-5 per group.

Figure 4. The loss of LPL in astrocytes causes ceramide accumulation, ER stress and increased immunoreactivity of iba1 and AGRP in the hypothalamus. Total ceramide content (A) and acyl-chain ceramide species (B) in the hypothalamus of GFAP-LPL^{+/+} and GFAP-LPL^{-/-} mice were determined by lipidomics (n=4 per group). The expression of ER stress markers (C) was examined in the hypothalamus of GFAP-LPL^{+/+} and GFAP-LPL^{-/-} mice (n=6-8 per group). No differences were found in the reactivity of GFAP in the hypothalamus (D&E); while microglial (iba-1 positive cells) reactivity was increased in GFAP-LPL^{-/-} mice (F&G) (n= 6-12 mice). POMC cell number did not change (H&I), whereas AGRP immunoreactivity was increased in the hypothalamus of GFAP-LPL^{-/-} mice (J&K) (n= 6-12 mice). GFAP: Glial fibrillary acidic protein. IBA1: ionized calcium-binding adapter molecule 1. AGRP: Agouti-related protein. POMC: Proopiomelanocortin. Atf4: activating transcription factor 4. Xbp1: X-box binding protein 1. Grp78: glucose-regulated protein 78 kDa. Chop: C/EBP-homologous protein. $p < 0.05$ for *. $p < 0.001$ for ***. Scale bar=100 μ m for (D-K).

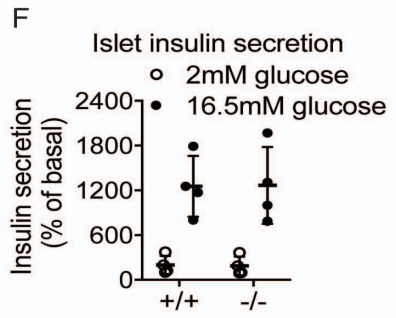
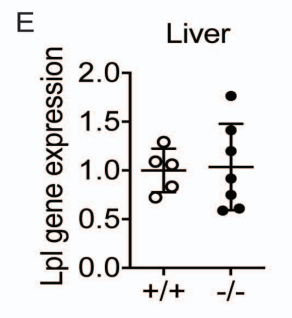
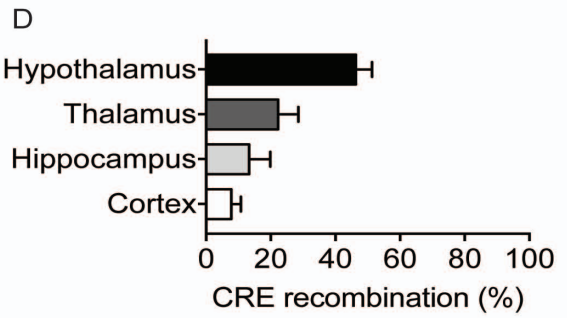
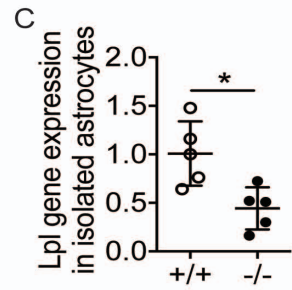
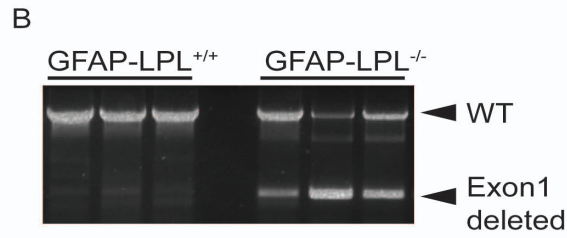
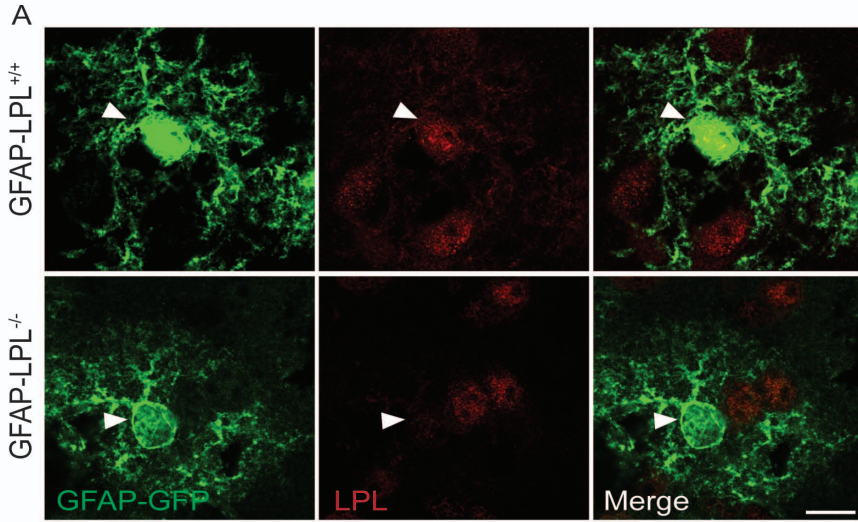
Figure 5. Mice lacking LPL in astrocytes have exaggerated body weight gain and glucose intolerance when maintained on HFD. GFAP-LPL^{-/-} mice fed on HFD had increased body weight gain (A), unchanged lean mass (B), increased fat mass (C) and increased daily food intake (D) compared with GFAP-LPL^{+/+} littermates. Calorimetric analysis demonstrated that GFAP-LPL^{-/-} mice had higher energy expenditure (E) and lower physical activity (F). Plasma leptin levels increased in GFAP-LPL^{-/-} mice (G); while plasma insulin levels were unchanged (H). GFAP-LPL^{-/-} mice had impaired glucose tolerance (I) and increased area under the curve (AUC) compared with GFAP-LPL^{+/+} littermates (J). $p < 0.05$ for *, $p < 0.01$ for **, $p < 0.001$ for. $n = 6-12$ mice for metabolic phenotyping and calorimetric study.

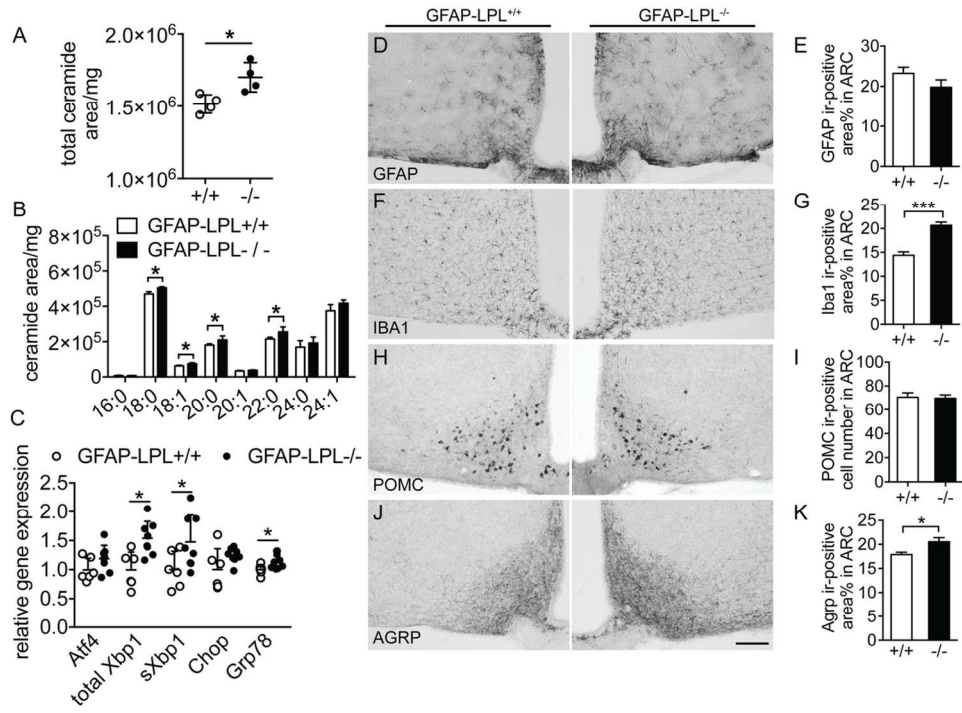


68x70mm (300 x 300 DPI)

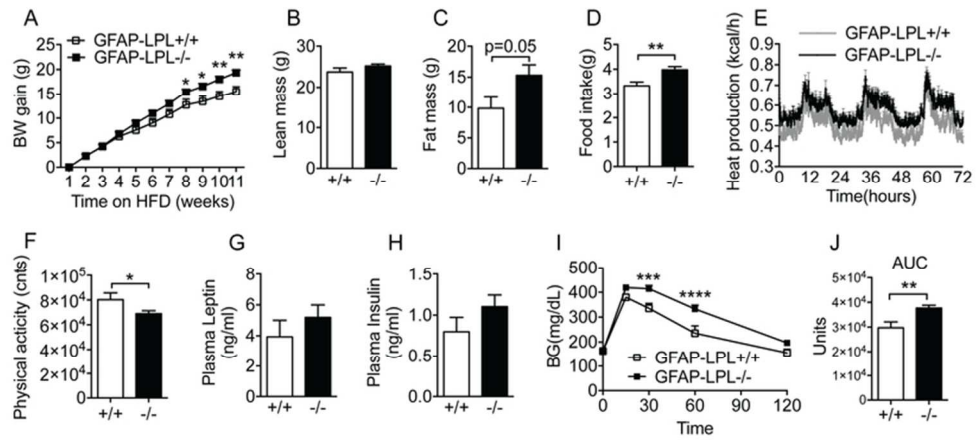


78x39mm (300 x 300 DPI)





117x83mm (300 x 300 DPI)



71x31mm (300 x 300 DPI)

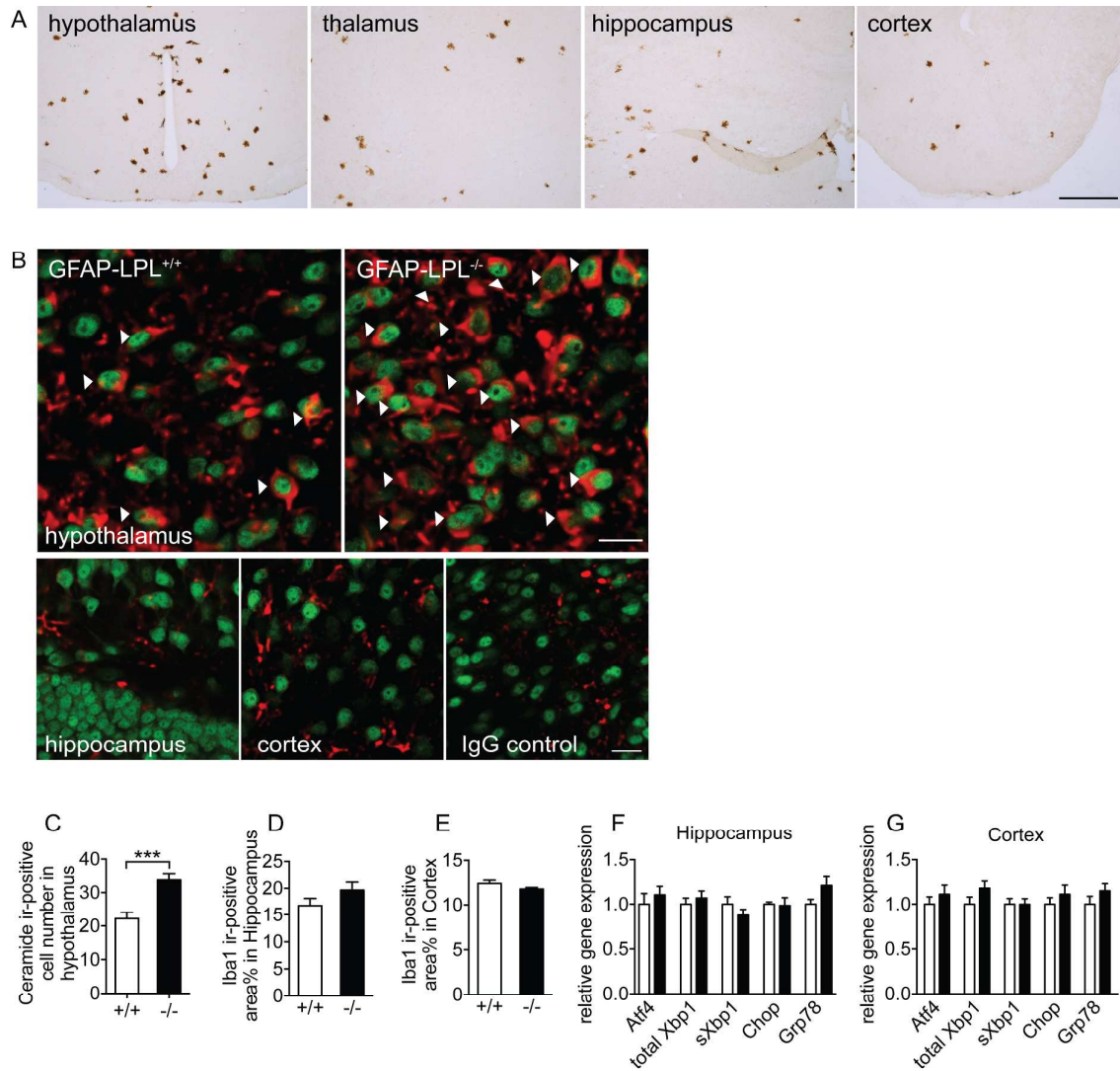
Online Supplemental Materials

Disruption of Lipid Uptake in Astroglia Exacerbates Diet Induced Obesity

Yuanqing Gao, Clarita Layritz, Beata Legutko, Thomas O Eichmann, Elise Laperrousaz, Valentine S Moullé, Celine Cruciani-Guglielmacci, Christophe Magnan, Serge Luquet, Stephen C Woods, Robert H Eckel, Chun-Xia Yi, Cristina Garcia-Caceres, Matthias H Tschöp

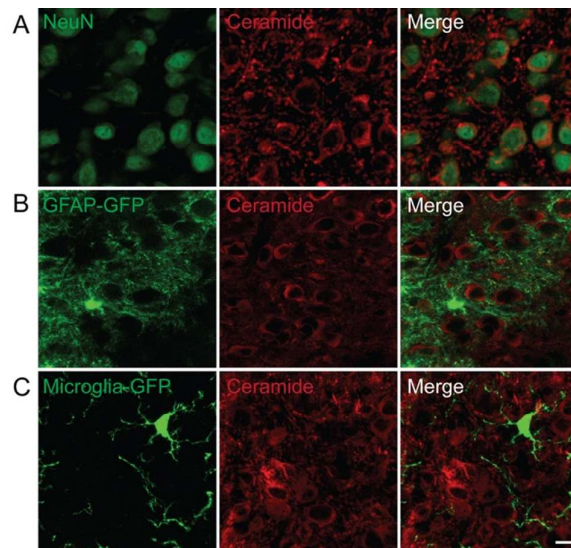
Figure:3

Table:1

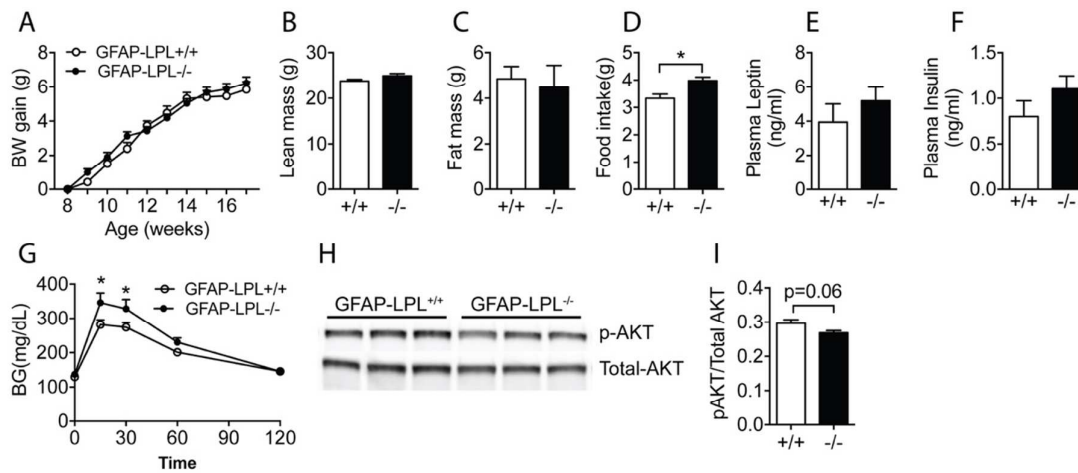


Supplemental Figure 1. Cre-mediated recombination, ceramide and microglia immunoreactivity and ER stress in different brain regions. The postnatal Cre-mediated recombination in distinct brain regions was shown by immunohistochemistry with anti-GFP antibody in GFAP-LPL^{+/+} adult mice crossed with Rosa26 ACTB-tdTomato reporter mice, 4 weeks after tamoxifen injection (A). Ceramide immunoreactivity is increased in GFAP-LPL^{-/-} hypothalamus but hardly detectable in hippocampus or cortex (ceramide, red dye, alexa 594; NeuN, green dye, alexa 488) (B). Quantification of ceramide immunoreactivity (-ir) in the hypothalamus (C) and iba1-ir in hippocampus and cortex (D & E). The expression of the

genes related with ER stress pathway was studied by qPCR in hippocampus and cortex (F & G). Scale bar: (A)= 500 μm and (B)= 20 μm . 6-12 animals for (C) – (G).



Supplemental Figure 2. The presence of ceramides in hypothalamic neurons. Positive co-localizations of ceramide (red dye, alexa 594) and NeuN (neuronal marker; green dye, alexa 488) were detected in the hypothalamus of wildtype adult mice (A). Ceramide positive cells (red dye) were undetectable in GFAP-expressing astrocytes (B) nor microglia (C) (GFP-positive cells; green dye) in the hypothalamus of hGFAP-eGFP or microglia-GFP reporter mice, respectively. GFAP: Glial fibrillary acidic protein; GFP: green fluorescence protein. Scale bar=10 μ m.



Supplemental Figure 3. Metabolic phenotype of GFAP-LPL^{+/+} and GFAP-LPL^{-/-} mice fed with a standard chow diet. On a standard chow diet, GFAP-LPL^{-/-} mice showed a higher daily food intake (D) without changes in body weight (BW) gain (A), lean mass (B) or fat mass (C) compared with their littermate controls. Plasma leptin (E) and insulin (F) levels were unchanged between groups. GFAP-LPL^{-/-} mice had worse glucose tolerance 8 weeks after tamoxifen injection (G). Western blotting depicting changes in p-AKT (phosphorylation of protein kinase B in Ser 473) and total-Akt in the hypothalamus of mice after 10 min of peripheral insulin injection (H). Western blot quantification of hypothalamic p-Akt/Akt levels in response to peripheral insulin injection in GFAP-LPL^{-/-} mice (I). $p < 0.05$ for *. n=8-9 mice per group for metabolic phenotyping.

Table 1. qRT-PCR SYBR primer sequences or taqman probes for amplification of cDNA

Gene symbol	Sequence (5' - 3')
Hprt	Mm01545399_m1
Hprt	GCAGTACAGCCCCAAAATGG
	AACAAAGTCTGGCCTGTATCCAA
Lpl	Mm00434764_m1
Fasn	MM00662319_m1
Cd36	Mm01135198_m1
sXbp1	CTGAGTCCGAATCAGGTGCAG
	GTCCATGGGAAGATGTTCTGG
totalXbp1	CAGCACTCAGACTATGTGCA
	GTCCATGGGAAGATGTTCTGG
Atf4	GGGTTCTGTCTTCCACTCCA
	AAGCAGCAGAGTCAGGCTTTC
Chop	CCACCACACCTGAAAGCAGAA
	AGGTGAAAGGCAGGGACTCA
Grp78	TTCAGCCAATTATCAGCAAACCTCT
	TTTTCTGATGTATCCTCTTCACCAGT